Journal of Zhejiang University-SCIENCE A (Applied Physics & Engineering)
ISSN 1673-565X (Print); ISSN 1862-1775 (Online)
www.zju.edu.cn/jzus; www.springerlink.com
E-mail: jzus@zju.edu.cn

# Chip morphology predictions while machining hardened tool steel using finite element and smoothed particles hydrodynamics methods*

Usama UMER†[1], Jaber Abu QUDEIRI[1], Mohammad ASHFAQ[1], Abdulrahman AL-AHMARI[1,2]

([1]*Princess Fatima Alnijiris's Research Chair for Advanced Manufacturing Technology (FARCAMT), Advanced Manufacturing Institute, King Saud University, Riyadh, Saudi Arabia*)

([2]*Industrial Engineering Department, College of Engineering, King Saud University, Riyadh, Saudi Arabia*)

†E-mail: usamaumer@yahoo.com

Received Jan. 18, 2016; Revision accepted June 17, 2016; Crosschecked Oct. 13, 2016

**Abstract:** Chip morphology predictions in metal cutting have always been challenging because of the complexity of the various multiphysical phenomena that occur across the tool-chip interface. An accurate prediction of chip morphology is a key factor in the assessment of a particular machining operation with regard to both tool performance and workpiece quality. Although finite element (FE) models are being developed over the last two decades, their capabilities in modeling correct material flow around the tool tip with shear localization are very limited. FE models with an arbitrary Lagrangian Eulerian (ALE) approach are able to simulate correct material flow around the tool tip. However, these models are unable to predict any shear localization based on material flow criteria. On the other hand, FE models with a Lagrangian formulation can simulate shear localization in the chip segments; they need to make use of a mesh-based chip separation criterion that significantly affects material flow around the tool tip. In this study a mesh-free method viz. smoothed particles hydrodynamics (SPH) is implemented to simulate shear localization in the chip while machining hardened steel. Unlike other SPH models developed by some researchers, this model is based on a renormalized formulation that can consider frictional stresses along the tool-chip interface giving a realistic chip shape and material flow. SPH models with different cutting parameters are compared with the traditional FE models and it has been found that the SPH models are good for predicting shear localized chips and do not need any geometric or mesh-based chip separation criteria.

**Key words:** Chip morphology, Finite element (FE), Smoothed particles hydrodynamics (SPH), Hardened tool steel, Serrated chips

http://dx.doi.org/10.1631/jzus.A1600023 **CLC number:** TG58

## 1 Introduction

With the growing need for high performance materials in different engineering disciplines, optimization of materials processing technologies is becoming ever more challenging. Out of many manufacturing processes, machining is considered to be the most complex because of the unconstrained flow of materials and the multi-disciplinary physics involved at different cutting speed regimes. One of the key performance identifiers in machining is the chip morphology. It is considered to be the most important because of its effect on cutting forces, temperatures, tool wear, and the surface integrity of the workpiece. Researchers have developed various analytical and numerical models for predicting chip morphology which are mostly based on the assumption of continuous chip formation or serrated chip formation. Models which are able to predict chip morphology

* Project supported by the King Saud University, Vice Deanship of Research Chairs, Saudi Arabia

ORCID: Usama UMER, http://orcid.org/0000-0001-8715-7905

transition are rare and a thorough understanding of the basic mechanism is required.

Most of the published work on the modeling of the machining operation is limited to continuous chip formation because of its stable nature and the ease with which it may be implemented in a numerical model. Serrated, shear localized or saw tooth chips contain alternating bands of low and high shear strains. It has been found that the intensity of shear bands increases with cutting speed. Usually there are threshold speeds for given cutting conditions at which transition occurs from continuous to serrated and from serrated to discontinuous chips.

Komanduri *et al.* (1982), Shaw (1984), and Hou and Komanduri (1997) did pioneer work in understanding the mechanism of chip formation while machining high strength alloy steels at high speeds. Experiments were performed on AISI 4340 alloy steel (16 to 53 HRC) at cutting speeds from 15 to 2500 m/min. Metallurgical examination revealed two types of chips, i.e., continuous and serrated at low and high cutting speeds, respectively. They concluded that the speeds at which shear-localized chips were formed depended on the properties of the work material.

Both cutting and thrust forces show a cyclic variation due to a varying chip load in machining with serrated chips. This leads to chatter and vibration in the system and ultimately leads to undesirable performance characteristics, i.e., excessive tool wear and poor surface integrity. In a low stiffness machining system this problem may become very severe due to self-excited vibrations. These occur due to coincidence of the chip load frequency and the natural frequency of the machining system. Tool-work piece interface temperatures are also higher in comparison with continuous chips, significantly affecting the tool's performance at high cutting speeds (Hou and Komanduri, 1997).

In view of the above, accurate prediction of chip morphology along with performance variables such as cutting forces, stress, and temperature distribution is needed. Serrated chip formulation in metal cutting has been modeled by many researchers with different numerical and material models. Most model serrated chips based on crack formation and propagation based on shear failure criteria while a few assume that shear localization occurs mainly due to thermal softening in a particular strain range. The phenomenon is termed adiabatic shear banding and mainly occurs due to the inability of some metals to strain harden at high strain rates. According to Bai and Dodd (1992) and other researchers (Guo and Yen, 2004; Gu *et al.*, 2013) both theories are not mutually exclusive and adiabatic shear bands follow crack formation and propagation. In addition to thermal softening, other phenomena have also been identified such as strain softening which occurs due to dynamic recrystallization and recovery and is responsible for the formation of saw tooth chips (Rhim and Oh, 2006; Calamaz *et al.*, 2008; Sima and Özel, 2010).

Various flow stress models have been utilized with and without failure criteria to model shear localized and saw tooth chip formation. The most widely used is the Johnson-Cook flow stress model which takes into account strain hardening, strain rate hardening, and thermal softening effects (Johnson and Cook, 1983). However, this model is unable to simulate serrated chip formation without any failure criterion and many researchers have used additional parameters to simulate adiabatic shear banding by incorporating phenomena such as strain softening because of dynamic recrystallization and recovery (Rhim and Oh, 2006; Calamaz *et al.*, 2008; Sima and Özel, 2010). While simulating serrated chips in AISI 1045, Rhim and Oh (2006) used two flow stress equations based on temperature ranges. They found that at above half the melting temperature dynamic recrystallization and recovery occur and they modified the corresponding flow stress equation to include this effect. Below half the melting temperature the standard Johnson-Cook model was employed.

Calamaz *et al.* (2008) used a modified Johnson-Cook model to include the strain rate effects. With this model the flow stress behaves in a similar manner as in the Johnson-Cook model up to a critical strain value. Beyond this the flow stress starts to decrease and finally becomes constant at higher strains. Sima and Özel (2010) also developed some modified Johnson-Cook models to include the strain rate effects. It has been found that a model similar to that of Calamaz *et al*. (2008) is in good agreement with experimental results. Researchers (Calamaz *et al.*, 2008; Sima and Özel, 2010) did not use any damage criterion for the simulation of serrated chips.

Umbrello *et al.* (2008) developed a hardness-based flow stress model for AISI H13 to model workpiece machining with different initial hardness.

The effect of changing hardness on cutting forces and chip segmentation was well captured by this model. The study utilized Cockcroft and Latham (1968)'s criterion to model crack formation and propagation to simulate serrated chips. Ceretti *et al.* (1999) modified a general purpose FE code DEFORM 2D to model segmented chips in AISI 1045. The cracks in the chips were simulated by an element deletion method based on a critical damage value. Hua and Shivpuri (2004) also applied the same methodology to simulate serrated chips in titanium alloys at various speeds.

Xie *et al.* (1998) developed a flow localization parameter that was able to predict the onset of shear localization in metal cutting. The simulation was done using an implicit 2D code and a node de-bond method was utilized to separate the chip from the work piece. The model was able to predict cutting forces, stress, and strain distribution. However, temperatures on the tool and workpiece were not presented. In contrast, Ng and Aspinwall (2002b) used an element deletion technique with Johnson-Cook shear failure criteria to simulate serrated chip formation in hardened steel. Another FE model was developed for continuous chip formation without any shear failure criterion. A comparative study has been presented by analyzing stress and temperature distributions in both types of chip formation. Arrazola *et al.* (2007) modeled serrated chips in AISI-4140 based on adiabatic shear banding phenomenon and did not consider any failure criteria. Their FE model was built using arbitrary Lagrangian Eulerian (ALE) approach and chip formation was modeled by deformation of the mesh only. However, in contrast to models based on a Lagrangian approach, these types of models are unable to obtain correct chip morphology.

In contrast to mesh-based FE models, research on a mesh-free method for serrated chip simulation is very limited. A mesh-free method, in particular smoothed particles hydrodynamics (SPH), offers various advantages over conventional FE models. Firstly, it does not need any mesh-based chip separation criteria such as element deletion or node splitting that are required in FE models. Secondly, there is no mesh distortion and no need for any adaptive meshing. Highly deformed and serrated chips can easily be simulated with this mesh-free method. In addition, this method does not need a predefined parting line, and hence tool penetration with different edge preparations can easily be modeled.

In this mesh-free method, material properties and field variables are evaluated at SPH particle locations. The particle movement depends on material deformation (Xi *et al.*, 2014). This makes the SPH method most suitable for high deformation processes as there is no excessive mesh tangling and distortion as in FE models. Mesh-based methods consider connectivity between nodes to form spatial derivatives. In contrast, the SPH method uses a kernel approximation which is based on disordered interpolation points, without any consideration of neighboring points, to form spatial derivatives. Details about the SPH formulation can be found in (Liu and Liu, 2010).

Limido *et al.* (2007) utilized the LS-DYNA SPH code to model continuous chip formation in aluminum alloy and serrated chip formation in hardened steel. The model predicted chip morphology and cutting forces with errors of 10% to 30%. The SPH models were built without any friction criterion which is not a correct approach, as the chip contact length and chip morphology are heavily dependent on the selected friction criterion. Madaj and Píška (2013) modeled orthogonal machining of aluminum A2024-T351 alloy using published experimental results. Serrated chips were simulated and the effects of Johnson-Cook damage model parameters and SPH density on cutting forces, chip morphology, plastic strain, and strain rates were discussed. Xi *et al.* (2014) used an SPH to model thermally assisted machining of Ti6Al4V alloy. The influences of initial workpiece temperature on chip formation and cutting forces were investigated. The model was able to simulate serrated chips at different speeds. However, the model seems to be developed with a default numerical formulation for SPH that gives rise to a very high tool-chip contact length and an unrealistic chip flow. Calamaz *et al.* (2009) developed 2D SPH models to investigate the effects of a worn tool on cutting forces and chip morphologies while machining Ti6Al4V alloy using a tungsten carbide tool. Two models, one with the new tool and the other with worn tools, were developed. The models utilized no friction and the cutting speed is set to 10 times the real cutting speed. These assumptions give rise to errors of around 25%. However, the models were able to predict reasonable variations of cutting and feed forces due to worn tools. Heisel *et al.* (2013) developed an SPH model to simulate the orthogonal machining of AISI 1045

steel. The study was based on the effects of various input parameters of the SPH solver on cutting forces and chip compression ratios, and suggested optimum input parameters after developing an objective function and optimization runs.

This paper describes mesh-based Lagrangian and mesh-free (SPH) models to simulate chip morphology transition in high strength alloy steel AISI H13 at a high cutting speed. It has been shown that the standard Johnson-Cook model with suitable damage parameters can be used quite satisfactorily to model serrated chips in AISI H13 based on crack formation and propagation criteria. This implies that a modified Johnson-Cook model is not always required to simulate serrated chip flow. In addition, both FE and SPH models are able to predict cutting forces and chip morphology changes with varying cutting speeds and feeds. The results from the models have been verified by high speed orthogonal cutting tests on AISI H13 tubes.

## 2 Experimental setup

The experiments were conducted using polycrystalline cubic boron nitride (PCBN) cutting inserts having a triangular shape with honed edge preparation of 0.02 mm and a nose radius of 1.2 mm as shown in Fig. 1.

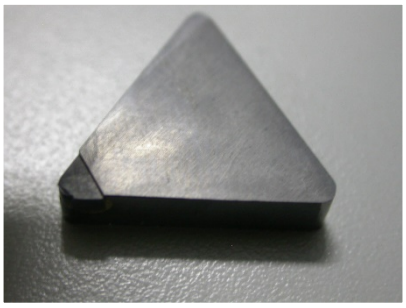

**Fig. 1 PCBN cutting insert used in the experiments**

The cutting insert along with the tool holder gives rake angle of −5° and clearance angle of 5°. The physical and mechanical properties of H13 and PCBN are shown in Table 1, while the cutting parameters are listed in Table 2. For cutting and thrust force measurement, a Kistler 9257B dynamometer with a charge amplifier was used. The system was equipped with a data acquisition program to collect the cutting force signals and save them for further analysis. An image of the experimental setup is shown in Fig. 2. The chip morphology examinations were carried out using scanning electron microscopy (SEM). The chip samples for SEM were prepared by grinding, polishing, and etching in a solution of 2% Nital.

**Table 1 Mechanical and physical properties of H13 and PCBN**

| Parameter | Value | |
|---|---|---|
| | H13 | PCBN |
| Density (kg/m$^3$) | 7800 | 3399.5 |
| Elastic modulus (GPa) | 211 | 652 |
| Poisson's ratio | 0.28 | 0.128 |
| Thermal conductivity (W/(m·K)) | 37 | 100 |
| Specific heat (J/(kg·K)) | 560 | 960 |
| Hardness (HRC) | 49 | – |

**Table 2 Cutting parameters for orthogonal cutting tests**

| Cutting speed, $V$ (m/min) | Feed rate, $f$ (mm/rev) | Depth of cut, $a_p$ (mm) |
|---|---|---|
| 150 | 0.15 | 2 |
| 200 | 0.15 | 2 |
| 250 | 0.15 | 2 |
| 150 | 0.25 | 2 |
| 200 | 0.25 | 2 |
| 250 | 0.25 | 2 |

**Fig. 2 Experimental setup to analyze and record cutting force data**

## 3 Chip formation modeling

### 3.1 Finite element model

The commercial finite element (FE) package ABAQUS/Explicit® (ABAQUS Analysis User Manual, 2010) was used to model serrated chip formation in high strength alloy steel. A 2D FE model

with plane strain assumption was employed to simulate orthogonal cutting experiments. Chip morphology transition in high strength alloy steel was modeled using a Lagrangian approach, i.e., the workpiece is fixed and the tool moves with the selected cutting speed. The feed rate was adjusted by the vertical penetration depth of the cutting tool with respect to the workpiece. Chip separation from the workpiece and crack formation in the chip was realized using an element deletion technique based on Johnson-Cook shear failure criterion (Kouadri *et al.*, 2013). Elements were deleted from the model when the equivalent plastic strain value reached a critical limit.

A total of around 4000 CPE4RT (continuum plain strain and reduced integration with temperature degree of freedom) elements were designed on the workpiece and the cutting tool for the FE model. An undeformed mesh for the cutting tool and workpiece is shown in Fig. 3. It can be seen that comparatively finer mesh was used for the chip part of the workpiece to account for high stresses and temperature gradients.

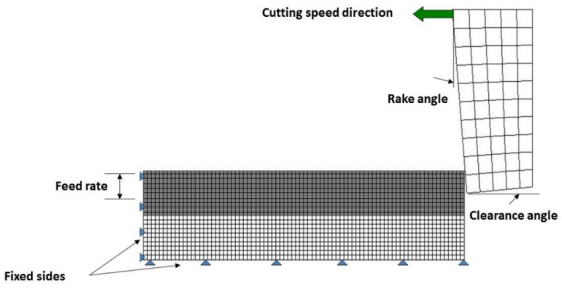


**Fig. 3 FE models for the workpiece and the cutting tool**

### 3.2 Smoothed particles hydrodynamics model

Since the tool was considered as rigid, only the workpiece was modeled with SPH particles. To model contact between FE (tool) and SPH (workpiece) parts, finer spacing is required. Contact is not recognized with coarse spacing. Therefore, a uniform spacing of 0.02 mm was used between the particles as shown in Fig. 4. As discussed later a renormalized formulation was used in all SPH models. In addition, all smoothing length parameters were set to default values. As with the FE model a sharp tool was utilized for all simulations. The default SPH formulation is unable to manipulate the correct particle distributions around the contact boundaries due to lack of neighboring particles. To overcome this problem an alternative formulation, called renormalized formulation, is proposed in LS-DYNA. This method is based on the work of Randles and Libersky (1996) and Vila (2005). With this method a better distribution of particles around the contact boundaries is obtained resulting in precise calculated quantities.

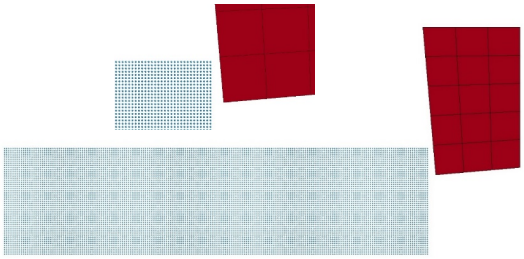

**Fig. 4 SPH models for the workpiece and the cutting tool**

All SPH models were run with renormalized formulation. The default SPH formulation gives very high tool-chip contact length and is unable to accommodate any frictional effects. Hence, this method results in an unrealistic chip flow. The difference in chip formation using default and renormalized formulations is shown in Fig. 5.

Although the distribution of particles around the rake face has been improved in the renormalized formulation, the flow of particles around the tool tip adjacent to the flank face shows a strange behavior. The particles stay away from the tool tip and flank face resulting in a gap of few microns. This problem can be solved using a honed tool edge which results in a more realistic material flow around the tool tip. The difference between using a sharp and honed tool edge is shown in Fig. 6. However, this approach results in an increase of computational time by around 30% due to the increase in contact area. In order to have a logical comparison with FE models a sharp tool was utilized in all SPH models for the prediction of stress and strain distributions.

All simulations were run on an Intel core I5 (3.1 GHz) processor with 16 GB random access memory (RAM). Computational time for SPH models was found to be very higher as compared with FE models. For example, an FE model with a cutting speed of 250 m/min and a cutting length of 4 mm requires approximately 75 min for completion using a single processor, whereas an equivalent SPH model requires almost 18 h for the same simulation. Using parallel processing with four processors the

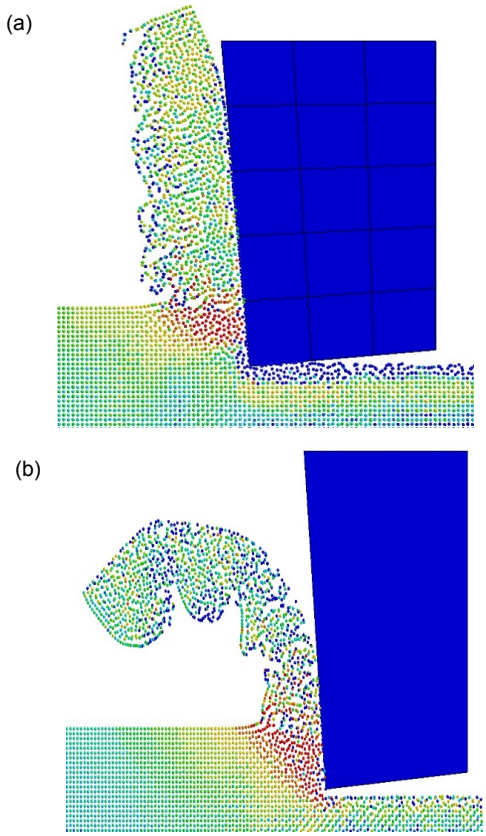


**Fig. 5 Difference in chip formation between default (a) and renormalized (b) SPH formulations**

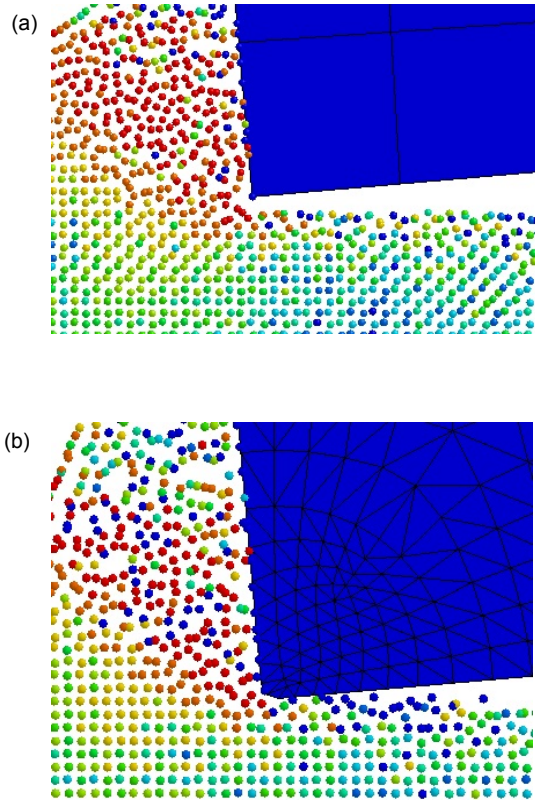


**Fig. 6 Material flow in SPH models around sharp (a) and honed edged (b) tools**

computational time reduces to 20 min for FE models. Parallel processing capabilities for FE-SPH contact formulation are not available in LS-DYNA.

### 3.3 Material flow and damage parameters for FE and SPH models

The workpiece material was represented by the Johnson-Cook plasticity model. The Johnson-Cook formulation involves the yield stress $\sigma$ at nonzero strain rate, strain hardening index $n$, equivalent plastic strain $\varepsilon$, equivalent plastic strain rate $\dot{\varepsilon}$, the melting temperature of the workpiece $T_{\text{melt}}$, operating temperature $T$, room temperature $T_{\text{room}}$, and strain rate sensitivity exponent $m$ as shown in Eq. (1). $B$ and $C$ are materials constants. The Johnson-Cook plasticity model is widely employed in high speed machining simulations as it can accommodate high strain rate and temperature effects. The Johnson-Cook parameters (Sartkulvanich *et al.*, 2004) for the workpiece materials are: $B$=981.7 MPa, $c$=0.023, $n$=0.182, $m$=2.7, and $T_{\text{melt}}$=1480 °C.

$$\sigma = B\varepsilon^{n}\left[1 + C\ln\left(\frac{\dot{\varepsilon}}{1000}\right)\right]\left[1 - \left(\frac{T - T_{\text{room}}}{T_{\text{melt}} - T_{\text{room}}}\right)^{m}\right]. \quad (1)$$

The chip separation in the workpiece was simulated using the Johnson-Cook damage law which takes into account strain, strain rate, temperature, and pressure (Sima and Özel, 2010). The damage was calculated for each element and is defined by

$$D = \sum \frac{\Delta\varepsilon}{\Delta\varepsilon_{\text{f}}}, \quad (2)$$

where $\Delta\varepsilon$ is the increment of equivalent plastic strain during an integration step, and $\Delta\varepsilon_{\text{f}}$ is the equivalent strain to fracture under the current conditions. Fracture is then allowed to occur when $D$=1.0 and the concerned elements are removed from the computation. The general expression for the fracture strain is given by

$$\varepsilon_{\mathrm{f}} = [D_1 + D_2 \exp(D_3 \sigma^*)]\left(1 + D_4 \ln \frac{\dot{\varepsilon}}{\dot{\varepsilon}_0}\right) \cdot \left[1 - D_5 \left(\frac{T - T_{\mathrm{room}}}{T_{\mathrm{melt}} - T_{\mathrm{room}}}\right)^m\right], \quad (3)$$

where $\dot{\varepsilon}_0$ is the reference strain rate and $\sigma^*$ is the ratio of pressure stress to von Mises stress. $D_1$ to $D_5$ are material constants and determined by tensile and torsion tests. The Johnson-Cook damage parameters for AISI H13 are: $D_1$=−0.8, $D_2$=2.1, $D_3$=−0.5, $D_4$=0.0002, and $D_5$=2.7.

### 3.4 Tool-chip interface characteristics for FE and SPH models

Zorev (1963)'s sliding-sticking friction model was utilized in the simulation. According to Zorev (1963), the division sliding and sticking region is given by (Ng and Aspinwall, 2002b)

$$\begin{cases} s = \mu p, & \mu p < \tau_{\max}, \\ s = \tau_{\max}, & \mu p \geq \tau_{\max}, \end{cases} \quad (4)$$

where $s$, $p$, and $\tau_{\max}$ are the friction, normal, and maximum equivalent shear stresses at the tool rake face, respectively. $\mu$ is the constant coefficient of friction, and $\mu$=0.3 was used in all simulations.

## 4 Results and discussion

### 4.1 Cutting force analysis

Typical cutting force signals from FE and SPH models are shown in Fig. 7. The variations in the cutting force signals correspond to the varying chip load due to segmented chips. The cutting forces at different cutting parameters from orthogonal cutting experiments along with FEM and SPH models results are depicted in Fig. 8. It can be seen that, for both feed rate values, cutting and thrust forces are not much effected by varying cutting speeds. With a feed rate of 0.25 mm/rev cutting forces ($F_c$) obtained are between 1200 and 1250 N, whereas the thrust forces ($F_t$) are found to be between 800 and 900 N (Fig. 8a). Decreasing the feed rate to 0.15 mm/rev results in a reduction of cutting forces by 40%, as shown in Fig. 8b, and a reduction of thrust forces by around 60%.

The predicted values of cutting forces and thrust forces from FEM and SPH models show similar trends. FEM models slightly overestimate the cutting and thrust forces with an average error of 5%. In contrast, SPH models show lower cutting forces. This may be due to different chip separation criteria used in the two models. Moreover, the penalty contact formulation between SPH and FE parts in LS-DYNA is significantly different from the default kinematic formulation in Abaqus/Explicit. This also results in reduced cutting forces. SPH models with sharp cutting tool are unable to predict thrust forces due to restricted material flow and need a honed edged tool for thrust force predictions. The average error for SPH models is around 8%.

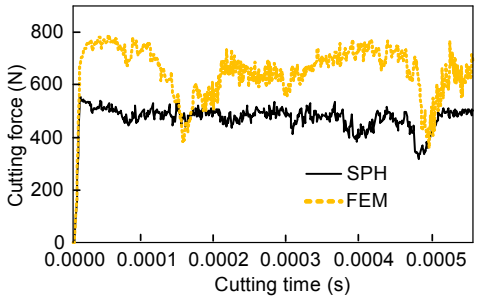


**Fig. 7 Cutting force signals from FE and SPH models at $V$=200 m/min and $f$=0.25 mm/rev**

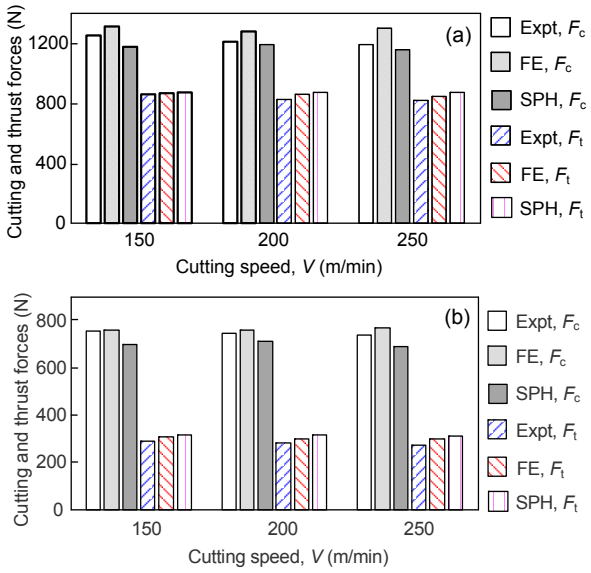


**Fig. 8 Cutting and thrust forces obtained at feed rate of 0.25 mm/rev (a) and 0.15 mm/rev (b)**

### 4.2 Chip morphology analysis

The chip morphologies obtained from FE and SPH models at a feed rate of 0.25 mm/rev with different cutting speeds are shown in Figs. 9 and 10, respectively. Serrated chips are predicted by both models and the frequency of serration increases with cutting speed. The SEM chip examination also reveals a similar pattern as shown in Fig. 11. Both FE and SPH models show that the length of cracks increases with the cutting speed. This is also confirmed by SEM photographs as shown in Fig. 11. These figures also show that the intensity of the cracks increases with the cutting speed which is also revealed in the SEM photograph. The chip curl increases with the cutting speed due to the increase in crack lengths.

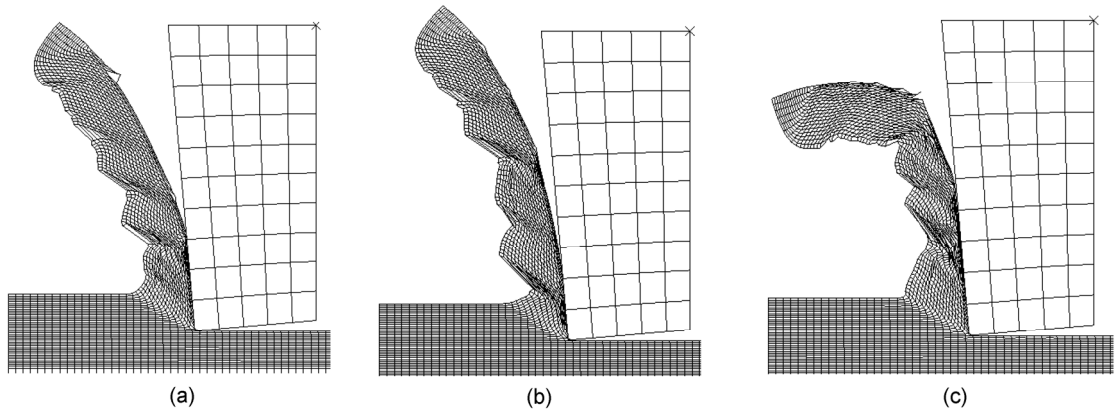


**Fig. 9 Chip morphologies from FE model at cutting speeds of 150 m/min (a), 200 m/min (b), and 250 m/min (c)**

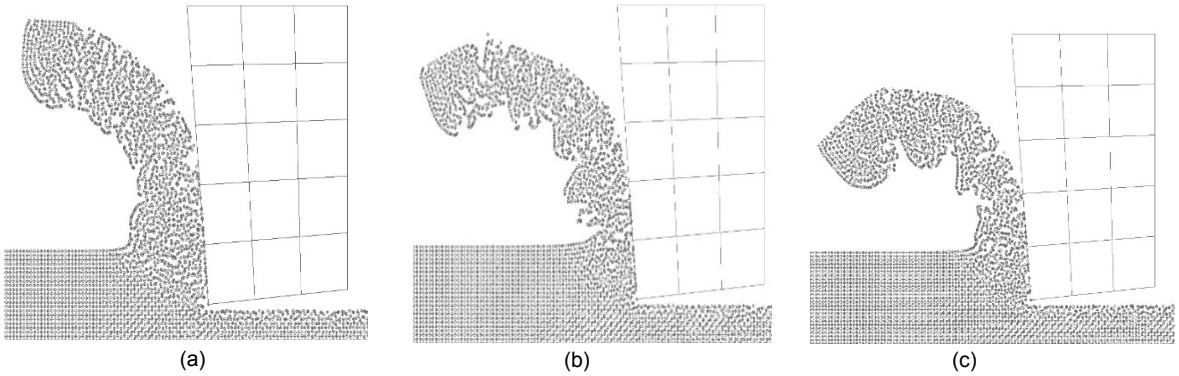


**Fig. 10 Chip morphologies from SPH model at cutting speeds of 150 m/min (a), 200 m/min (b), and 250 m/min (c)**

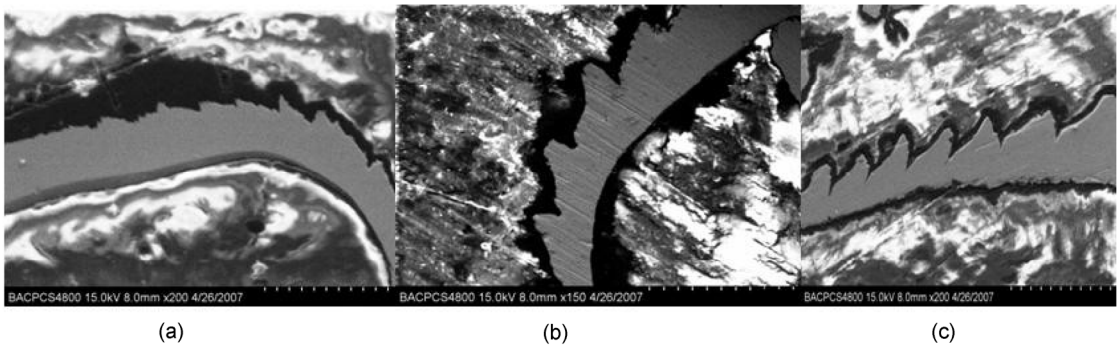


**Fig. 11 SEM photographs of serrated chips at cutting speeds of 150 m/min (a), 200 m/min (b), and 250 m/min (c)**

This is also reported by Ng and Aspinwall (2002b). Chip morphologies for the SPH models also show similar trends. However, the chip curl is greater due to higher deformability of the mesh-free workpiece. Serrated chip morphology can be described quantitatively through three parameters viz. peak, valley, and spacing as shown in Fig. 12. A comparative analysis of the average values of the parameters in Fig. 13 shows a reasonable agreement with experimental results for both models.

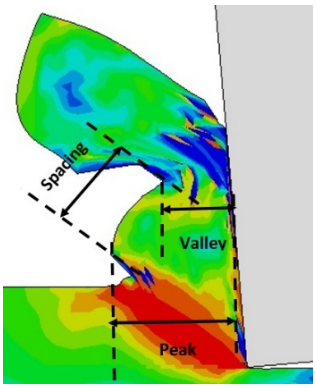


**Fig. 12 Serrated chip morphology parameters**

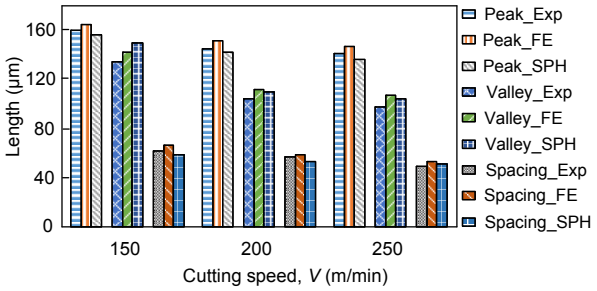


**Fig. 13 Serrated chip morphology parameters by experiments and models at feed rate of 0.25 mm/rev**

Another way to quantify chip segmentation was introduced by Atlati *et al.* (2011) using a segment intensity ratio (SIR). SIR is defined as the ratio of average plastic strain inside the shear band to the average plastic strain outside the shear band, i.e., $\mathrm{SIR}=\dfrac{\varepsilon_{\mathrm{in}}}{\varepsilon_{\mathrm{out}}}$.

It has been found that with high shear localization, the plastic strain inside the shear band increases and outside the band decreases giving rise to a high SIR value. In the present study, SIRs for FE and SPH models are calculated and it has been found that SIR increases slightly with the cutting speed as shown in Fig. 14. This is in accordance with the studies conducted by Atlati *et al.* (2011) and Kouadry *et al.* (2013).

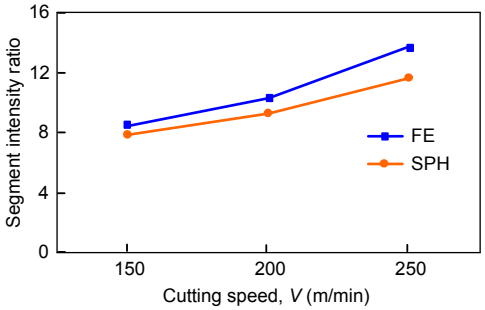


**Fig. 14 Segment intensity ratios (SIRs) at different cutting speeds ($f$=0.25 mm/rev)**

Figs. 15 and 16 also show von Mises stress contours for FE and SPH models, respectively. Both models show similar stress pattern with the highest von Mises stress at the primary shear zone and cyclic variation of stresses along the chip segments. As with the cutting forces, stresses are not much varying with the cutting speed and are almost constant. Reduction in feed rate leads to increases in stresses for both models as shown in Figs. 15 and 16. This mainly accounts for the size factor due to increase in specific cutting energy at lower feed values (Shaw, 1984). In comparison to FE models, SPH models show low stresses due to mesh free nature of the workpiece. The length of cracks decreases when the feed rate is reduced to 0.15 mm/rev as shown in Figs. 15 and 16.

Temperature contour at the workpiece and cutting tool is shown in Fig. 17a. Temperatures are the highest at the tool-chip interface and are between 700 and 720 °C. Unlike continuous chips, temperatures are not uniform and are higher in the chip segments due to slow heat transfer at higher cutting speeds. Fig. 17b shows that temperatures are increasing with the cutting speed and feed rate. No experiments were performed to verify the results, however, the range of temperatures and behavior predicted by FE models are in agreement with similar studies on high speed turning of H13 (Ng *et al.*, 1999; Ng and Aspinwall, 2002a; 2002b). Only FE models are able to predict temperatures as the SPH solver utilized in this study is unable to perform coupled temperature displacement analysis.

Fig. 18 shows equivalent plastic strain contour at feed rate of 0.25 mm/rev and cutting speed of 250 m/min obtained with FE and SPH models. Both models show a repeating pattern for equivalent plastic strain values and are comparatively higher at the shear bands between the chip segments. In contrast, Fig. 19 shows a uniform and low equivalent plastic strain contour at a cutting speed of 50 m/min for both FE and SPH models. Similar findings were reported by Arrazola *et al.* (2007) while modeling machining of

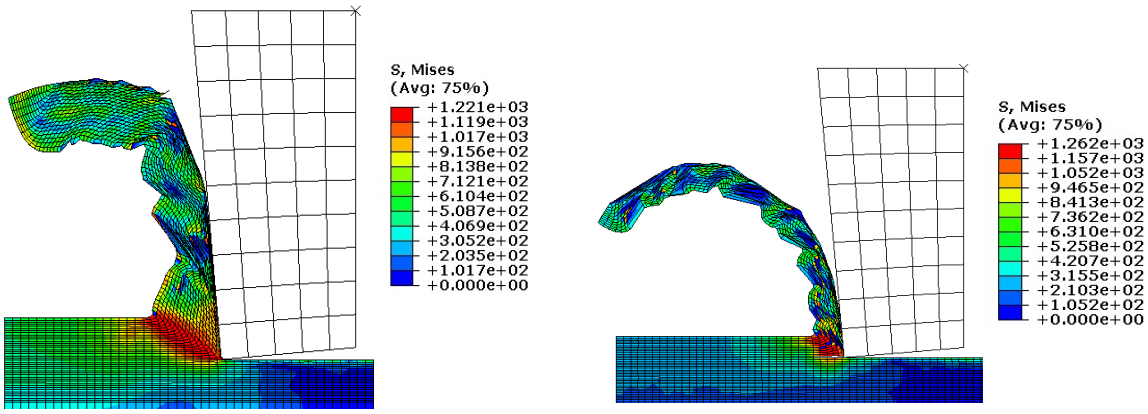


**Fig. 15 von Mises stress for FE model at feed rate of 0.25 mm/rev (a) and 0.15 mm/rev (b) (cutting speed is 250 m/min)**

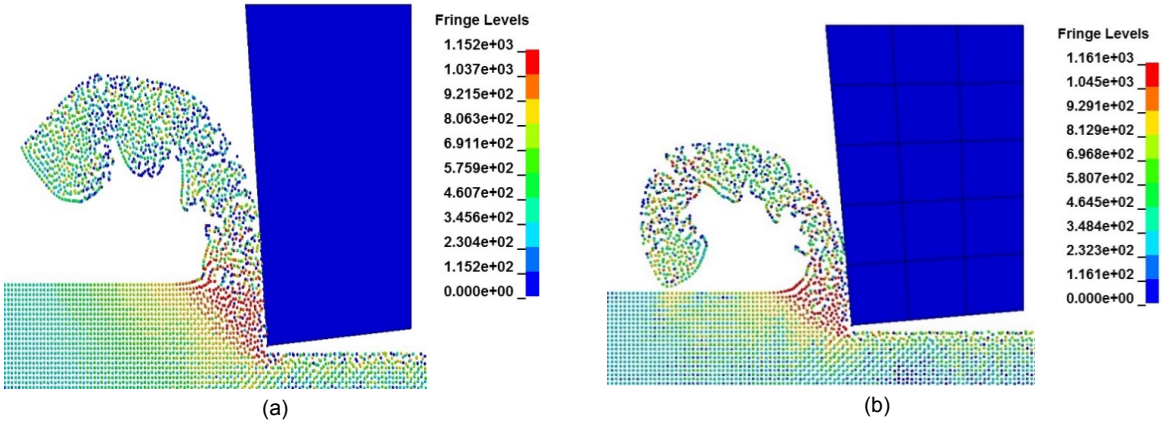


**Fig. 16 von Mises stress for SPH model at feed rate of 0.25 mm/rev (a) and 0.15 mm/rev (b) (cutting speed is 250 m/min)**

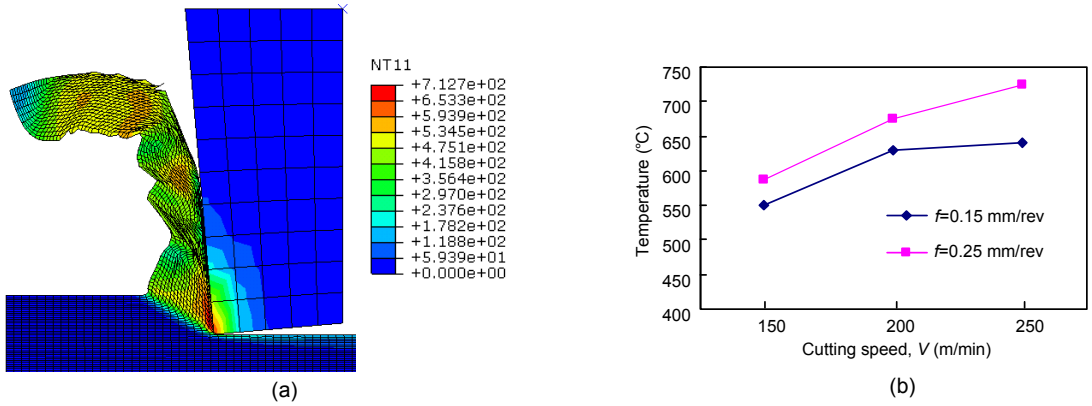


**Fig. 17 Temperature contour at cutting speed of 250 m/min and feed rate of 0.25 mm/rev (a); Variation in tool-chip interface temperature with cutting speeds and feed rates (b)**

AISI 4140 using the ALE approach. SPH models also show similar pattern with low values of equivalent plastic strain as compared with FE models.

The FE and SPH models developed for serrated chip formation are able to predict chip morphology changes from continuous to serrated and from serrated to discontinuous chips as shown in Figs. 19 and 20. Fig. 19 shows continuous chip formation at low cutting speed while Fig. 20 shows discontinuous chips formed at high cutting speed of 400 m/min.

## 5 Conclusions

1. The FE and SPH models developed in this study can simulate chip morphology and other process variables with reasonable degree of accuracy.

2. Serrated chips are observed in the cutting speed range of 150 to 250 m/min and they are successfully simulated by FE and SPH models.

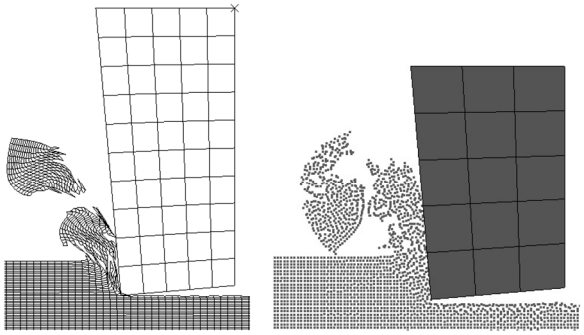


**Fig. 20 Discontinuous chip at cutting speed of 400 m/min with FE (a) and SPH (b) models**

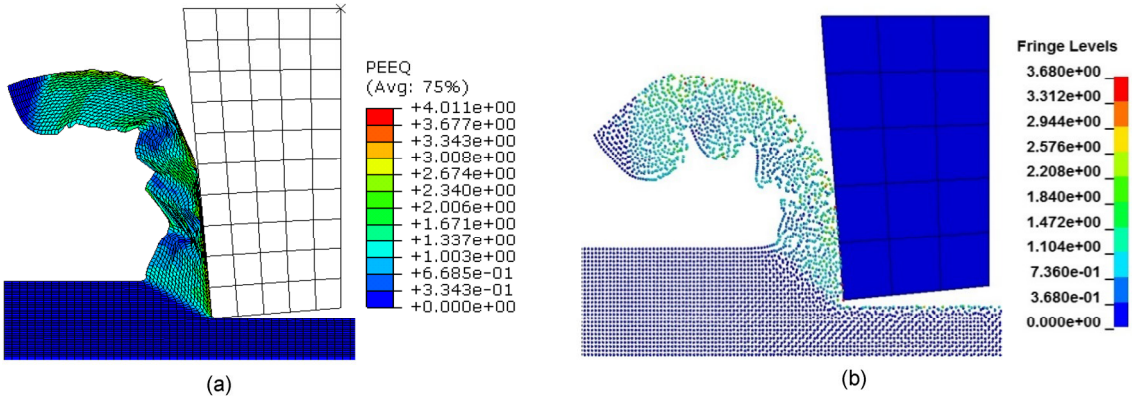


**Fig. 18 Equivalent plastic strain contour for FE (a) and SPH (b) models at cutting speed of 250 m/min (feed rate is 0.25 mm/rev)**

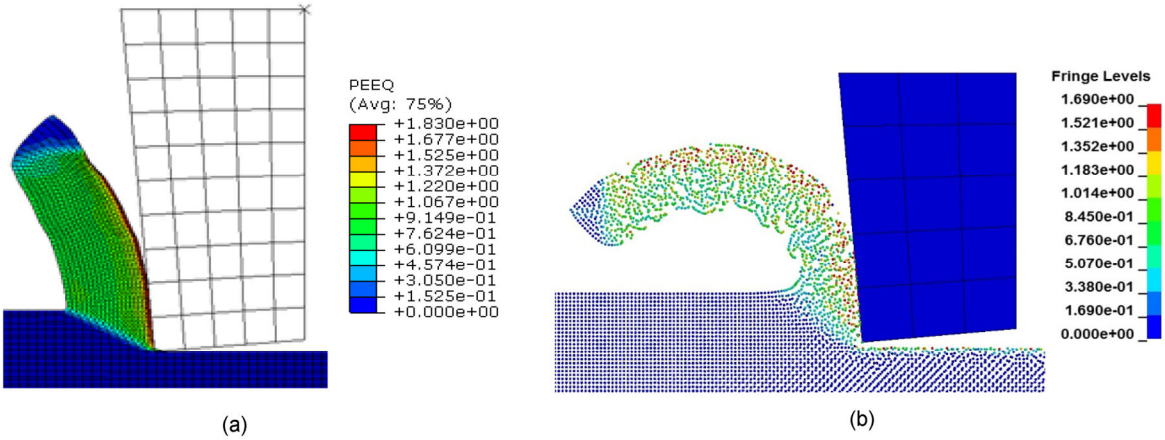


**Fig. 19 Equivalent plastic strain contour for FE (a) and SPH (b) models at cutting speed of 50 m/min (feed rate is 0.25 mm/rev)**

3. Cutting forces in the high speed range are mostly unaffected by change in cutting speed. On the other hand feed rate has marked effect on cutting forces which is also predicted by FE and SPH models with an average error of around 5% and 8%, respectively.

4. The SPH and FE models can predict chip morphology changes from continuous to segmented and from segmented to discontinuous chips by varying the cutting speed.

5. SPH models are able to simulate the correct stress and strain distributions with no need for a geometric or mesh-based chip separation criteria.

6. Tool edge preparation can be modeled with SPH method as it does not need any mesh-based chip separation criterion.

7. SPH models show low cutting forces and high chip curl as compared with FE models when using similar sets of material and friction parameters.

## References


ABAQUS Analysis User Manual, 2010. ABAQUS Documentation, V6.10. Dassault Systemes, France.

Arrazola, P.J., Villar, A., Ugarte, D., *et al.*, 2007. Serrated chip prediction in finite element modeling of the chip formation process. *Machining Science and Technology*, **11**: 367-390.

Atlati, S., Haddag, B., Nouari, M., *et al*., 2011. Analysis of a new segmentation intensity ratio "SIR" to characterize the chip segmentation process in machining ductile metals. *International Journal of Machine Tools and Manufacture*, **51**(9):687-700. http://dx.doi.org/10.1016/j.ijmachtools.2011.05.007

Calamaz, M., Coupard, D., Girot, F., 2008. A new material model for 2D numerical simulation of serrated chip formation when machining titanium alloy Ti–6Al–4V. *International Journal of Machine Tools and Manufacture*, **48**(3-4):275-288. http://dx.doi.org/10.1016/j.ijmachtools.2007.10.014

Calamaz, M., Limido, J., Nouari, M., *et al*., 2009. Toward a better understanding of tool wear effect through a comparison between experiments and SPH numerical modelling of machining hard materials. *International Journal of Refractory Metals and Hard Materials*, **27**(3): 595-604. http://dx.doi.org/10.1016/j.ijrmhm.2008.09.005

Ceretti, E., Lucchi, M., Altan, T., 1999. FEM simulation of orthogonal cutting: serrated chip formation. *Journal of Materials Processing Technology*, **95**(1-3):17-26. http://dx.doi.org/10.1016/S0924-0136(99)00261-7

Cockcroft, M.G., Latham, D.J., 1968. Ductility and the workability of metals. *Journal of the Institute of Metals*, **96**(1):33-39.

Dodd, B., 1992. Adiabatic Shear Localization: Occurrence, Theories, and Applications. Pergamon Press, Oxford, UK.

Gu, L.Y., Wang, M.J., Duan, C.Z., 2013. On adiabatic shear localized fracture during serrated chip evolution in high speed machining of hardened AISI 1045 steel. *International Journal of Mechanical Sciences*, **75**:288-298. http://dx.doi.org/10.1016/j.ijmecsci.2013.07.004

Guo, Y.B., Yen, D.W., 2004. A FEM study on mechanisms of discontinuous chip formation in hard machining. *Journal of Materials Processing Technology*, **155-156**:1350-1356. http://dx.doi.org/10.1016/j.jmatprotec.2004.04.210

Heisel, U., Zaloga, W., Krivoruchko, D., *et al.*, 2013. Modelling of orthogonal cutting processes with the method of smoothed particle hydrodynamics. *Production Engineering*, **7**(6):639-645. http://dx.doi.org/10.1007/s11740-013-0484-0

Hou, Z.B., Komanduri, R., 1997. Modeling of thermomechanical shear instability in machining. *International Journal of Mechanical Sciences*, **39**(11):1273-1314. http://dx.doi.org/10.1016/S0020-7403(97)00017-9

Hua, J., Shivpuri, R., 2004. Prediction of chip morphology and segmentation during the machining of titanium alloys. *Journal of Materials Processing Technology*, **150**(1-2): 124-133. http://dx.doi.org/10.1016/j.jmatprotec.2004.01.028

Johnson, G.R., Cook, W.H., 1983. A constitutive model and data for metals subjected to large strains, high strain rates and high temperatures. Proceedings of the 7th International Symposium on Ballistics, Hague, The Netherlands, **21**:541-547.

Komanduri, R., Schroeder, T., Hazra, J., *et al*., 1982. On the catastrophic shear instability in high-speed machining of an AISI 4340 steel. *Journal of Engineering for Industry*, **104**(2):121-131. http://dx.doi.org/10.1115/1.3185807

Kouadri, S., Necib, K., Atlati, S., *et al*., 2013. Quantification of the chip segmentation in metal machining: application to machining the aeronautical aluminium alloy AA2024-T351 with cemented carbide tools WC-Co. *International Journal of Machine Tools and Manufacture*, **64**:102-113. http://dx.doi.org/10.1016/j.ijmachtools.2012.08.006

Limido, J., Espinosa, C., Salaün, M., *et al.*, 2007. SPH method applied to high speed cutting modelling. *International Journal of Mechanical Sciences*, **49**(7):898-908. http://dx.doi.org/10.1016/j.ijmecsci.2006.11.005

Liu, M.B., Liu, G.R., 2010. Smoothed particle hydrodynamics (SPH): an overview and recent developments. *Archives of Computational Methods in Engineering*, **17**(1):25-76. http://dx.doi.org/10.1007/s11831-010-9040-7

Madaj, M., Píška, M., 2013. On the SPH orthogonal cutting simulation of A2024-T351 alloy. *Procedia CIRP*, **8**:152-157. http://dx.doi.org/10.1016/j.procir.2013.06.081

Ng, E.G., Aspinwall, D.K., 2002a. The effect of workpiece hardness and cutting speed on the machinability of AISI

H13 hot work die steel when using PCBN tooling. *Journal of Manufacturing Science and Engineering*, **124**(3):588-594. http://dx.doi.org/10.1115/1.1452749

Ng, E.G., Aspinwall, D.K., 2002b. Modelling of hard part machining. *Journal of Materials Processing Technology*, **127**(2):222-229. http://dx.doi.org/10.1016/S0924-0136(02)00146-2

Ng, E.G., Aspinwall, D.K., Brazil, D., *et al*., 1999. Modelling of temperature and forces when orthogonally machining hardened steel. *International Journal of Machine Tools and Manufacture*, **39**(6):885-903. http://dx.doi.org/10.1016/S0890-6955(98)00077-7

Randles, P.W., Libersky, L.D., 1996. Smoothed particle hydrodynamics: some recent improvements and applications. *Computer Methods in Applied Mechanics and Engineering*, **139**(1-4):375-408. http://dx.doi.org/10.1016/S0045-7825(96)01090-0

Rhim, S.H., Oh, S.I., 2006. Prediction of serrated chip formation in metal cutting process with new flow stress model for AISI 1045 steel. *Journal of Materials Processing Technology*, **171**(3):417-422. http://dx.doi.org/10.1016/j.jmatprotec.2005.08.002

Sartkulvanich, P., Koppka, F., Altan, T., 2004. Determination of flow stress for metal cutting simulation–a progress report. *Journal of Materials Processing Technology*, **146**(1):61-71. http://dx.doi.org/10.1016/S0924-0136(03)00845-8

Shaw, M.C., 1984. Metal Cutting Principles. Clarendon Press, Oxford, UK.

Sima, M., Özel, T., 2010. Modified material constitutive models for serrated chip formation simulations and experimental validation in machining of titanium alloy Ti–6Al–4V. *International Journal of Machine Tools and Manufacture*, **50**(11):943-960. http://dx.doi.org/10.1016/j.ijmachtools.2010.08.004

Umbrello, D., Rizzuti, S., Outeiro, J.C.C., *et al*., 2008. Hardness-based flow stress for numerical simulation of hard machining AISI H13 tool steel. *Journal of Materials Processing Technology*, **199**(1-3):64-73. http://dx.doi.org/10.1016/j.jmatprotec.2007.08.018

Vila, J., 2005. SPH renormalized hybrid methods for conservation laws: applications to free surface flows. *Lecture Notes in Computational Science & Engineering*, **43**:207-229. http://dx.doi.org/10.1007/3-540-27099-X_12

Xi, Y., Bermingham, M., Wang, G., *et al*., 2014. SPH/FE modeling of cutting force and chip formation during thermally assisted machining of Ti6Al4V alloy. *Computational Materials Science*, **84**:188-197. http://dx.doi.org/10.1016/j.commatsci.2013.12.018

Xie, J.Q., Bayoumi, A.E., Zbib, H.M., 1998. FEA modeling and simulation of shear localized chip formation in metal cutting. *International Journal of Machine Tools and Manufacture*, **38**(9):1067-1087. http://dx.doi.org/10.1016/S0890-6955(97)00063-1

Zorev, N.N., 1963. Inter-relationship between shear processes occurring along tool face and shear plane in metal cutting. *International Research in Production Engineering*, **49**:143-152.

## 中文概要

**题　目：基于有限元和光滑粒子流体动力学的硬质工具钢切屑形貌预测方法研究**

**目　的：**获得有效的高精度切屑形貌仿真方法。

**创新点：**通过比较不同切削参数下采用光滑粒子流体动力学模型和有限元模型仿真获得的切屑形貌，证明光滑粒子流体动力学模型可以很好地实现对节状切屑的仿真，而不需要额外的几何或基于网格的切屑分离准则。

**方　法：**基于有限元和光滑粒子流体动力学的切削形貌仿真方法。

**结　论：**通过比较不同切削参数下采用光滑粒子流体动力学模型和有限元模型仿真获得的切屑形貌，证明了基于裂纹形成与扩展理论，采用合理疲劳参数的标准 Johnson-Cook 模型完全可以实现对节状切屑形成过程的仿真，也即无需采用修正的 Johnson-Cook 模型。同时证明了有限元模型和光滑粒子流体动力学方法均可满足不同切削速度和进给量条件下的切削力和切屑形貌仿真。

**关键词：**切屑形貌；有限元；光滑粒子流体动力学；淬硬工具钢；锯齿形切屑